



ELSEVIER

Earth and Planetary Science Letters 179 (2000) 503–516

EPSL

www.elsevier.com/locate/epsl

# Evidence for Early Cretaceous oceanic crust trapped in the Philippine Sea Plate

A. Deschamps<sup>a,\*</sup>, P. Monié<sup>a</sup>, S. Lallemand<sup>a</sup>, S.-K. Hsu<sup>b</sup>, K.Y. Yeh<sup>c</sup>

<sup>a</sup> *Laboratoire de Géophysique, Tectonique et Sédimentologie, UMR 5573, Université Montpellier II, Place E. Bataillon, 34095 Montpellier Cedex 5, France*

<sup>b</sup> *Institute of Geophysics, National Central University, Chungli, Taiwan, PR China*

<sup>c</sup> *Geology Department, National Museum of Natural Science, Taiwan, PR China*

Received 24 January 2000; accepted 20 April 2000

## Abstract

The Huatung Basin is a small oceanic basin located east of Taiwan. Previous age estimates from magnetic lineation studies indicated an Eocene age for the basin, and formation from the Central Basin Spreading Center of the West Philippine Basin during the last phase of spreading in Middle Eocene. New Ar/Ar ages obtained on gabbros dredged on oceanic basement highs of the Huatung Basin are Early Cretaceous. These old ages are consistent with Early Cretaceous ages determined on radiolarian assemblages from Lanyu Island (Luzon Arc). We have performed magnetic anomalies modeling for an Early Cretaceous oceanic crust. Our results are in good agreement with new Ar/Ar ages determinations. The best fit is indeed obtained with an opening of the Huatung Basin during the Early Cretaceous from 131 to 119 Ma, with a half spreading rate varying between 25 and 30 mm/yr. The spreading center appears to be located south of the actual basin. The abnormal depth (5500 m instead of 5900 m) and thickness (~12 km instead of 6 km) of the crust beneath the basin indicate that there was probably an excess supply of magma during its formation. We propose that the basin is a fragment of the former 'proto-south China Sea' or possibly the 'New Guinea Basin' that has been trapped by the Philippine Sea Plate. © 2000 Elsevier Science B.V. All rights reserved.

*Keywords:* Taiwan; oceanic crust; Ar-40/Ar-39; Philippine Sea Plate; magnetic anomalies

## 1. Introduction

The Philippine Sea Plate (PSP) is a small plate sandwiched between the converging Eurasian and Pacific plates. The PSP consists of three back-arc basins which have been tectonically inactive since the Oligocene–Miocene: the West Philippine Ba-

sin (WPB), the Shikoku Basin and the Parece Vela Basin. These basins are dated, respectively, 56–33 [1], 23–15 and 29–15 Ma [2]. The Mariana Trough has been opening for 6 Ma [3]. The PSP is converging towards the Eurasian plate at a rate of 68 mm/yr in a direction of 309°N near Taiwan [4]. In this region, the oceanic crust of the WPB is subducting along the Ryukyu Trench. The oceanic nature of the crust is attested to by its depth and the existence of magnetic lineations [1,5,6], seismic-refraction data [7] and deep sea drilling [8].

\* Corresponding author. Fax: +33-4-67-52-39-08;  
E-mail: deschamp@dstu.univ-montp2.fr

The Huatung Basin located east of Taiwan constitutes the westernmost part of the PSP. It is bordered by the Luzon volcanic arc to the west and by the Gagua Ridge to the east (Fig. 1). It extends from latitude 20°30'N to 23°30'N, and from longitude 121°30'E to 123°E, and covers an area of about 22 300 km<sup>2</sup>.

The ages of the volcanic rocks in the northern Luzon arc range between 29 Ma [9] and present [10]. Nevertheless the occurrence of Upper Cretaceous to Eocene volcanic rocks in Luzon and in the eastern Philippines is well-known [11,12]. Recent studies have suggested that the Gagua Ridge bounding the Huatung Basin to the east formed during the Eocene, soon after the creation of the adjacent WPB crust [13].

Since no deep sea hole has been drilled in the Huatung Basin, the identification of the magnetic anomalies provide the most important constraint on the age of the seafloor. Hilde and Lee [1] initially recognized E–W trending magnetic lineations. They identified magnetic anomalies 19 to 16 indicating an age for the seafloor of the Huatung Basin ranging between 44 and 39 Ma old when using the reversal time scale model of Labrecque et al. [14] or between 41 to 36 Ma according to the new time scale of Cande and Kent [15]. Hilde and Lee [1] combined analyses of the magnetic lineations and seafloor structures of the WPB. They found that the WPB formed by spreading from the Central Basin Spreading Center in two distinct spreading phases. From 60 to 45 Ma, spreading was NE–SW (relative to present orientation), and from 45 to 35 Ma, spreading was N–S. They correlated the magnetic anomalies in the Huatung Basin with the E–W lineations created during the last spreading phase of the WPB during the Late Eocene.

Recently, ages for the Huatung Basin have been deduced from magnetic anomalies studies, confirming its Eocene age but with slight variations in the age window: 45 to 35 Ma for Kao et al. [16], 43 to 38 Ma for Lee et al. [17]. These authors assume that the basin formed at the Central Basin Spreading Center of the WPB in the southern hemisphere, is in good accordance with paleomagnetic data [18]. On the other hand, based on the assumption that the Huatung Basin formed in the

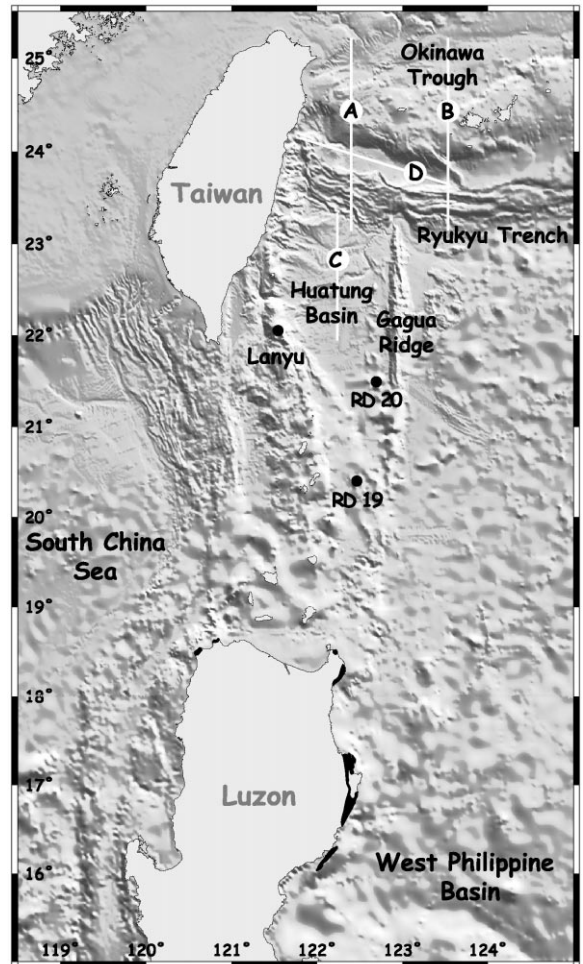


Fig. 1. Geodynamic setting of the Huatung Basin. The base-map is made with bathymetric data of [44]. The three black circles correspond to the location where early Cretaceous rocks have been discovered. A and B mark the location of the two N–S vertical sections with hypocenter locations shown on Fig. 7. C is the location of the seismic reflection profile shown on Fig. 5. D corresponds to the location of the crustal velocity model (Fig. 6). Black areas correspond to Early Cretaceous ophiolites.

northern hemisphere at 23°N, Sibuet et al. [19] assigned chrons 20 to 23 to the anomalies in the basin. They affirm that the basin belongs to a different plate than WPB, the Taiwan Sea Plate. This plate would have formed in two different spreading episodes between 51 and 15 Ma, but its youngest portion is considered to have already been subducted beneath the Ryukyu Trench, ex-

plaining why only its oldest part (51 to 43 Ma) is currently observed. However, the correlation of observed profiles with a magnetic model is non-unique because the width of the basin is less than 150 km and the number of available N–S magnetic profiles is therefore restricted. Moreover, although the E–W orientation of the magnetic lineations in the Huatung Basin is well determined [20], the number of magnetic polarity reversals is not sufficient to determine reliable ages, as shown by the various attempts at age determination from the magnetic lineations. The origin and age of the Huatung Basin are therefore still controversial. The goal of this paper is to examine the implications of new dating of rocks which have been dredged in the basin.

## 2. $^{40}\text{Ar}/^{39}\text{Ar}$ and K–Ar dating of gabbros from the Huatung Basin

Gabbros were dredged in the Huatung Basin at two sites from the western flank of the Gagua Ridge during the R/V *Vema* cruise V3609 in 1980 [21,22]. The location of the two sites is: 20.40°N/121.47°E (site RD19) and 21.49°N/122.69°E (site RD20) (Fig. 1). Among the various gabbros collected at these sites, two samples from site RD19 and one sample from site RD20 were selected after careful microscopic examination and elimination of altered rocks. Single grains of amphibole from these three samples were analyzed by the  $^{40}\text{Ar}/^{39}\text{Ar}$  laser-probe dating technique.

### 2.1. $^{40}\text{Ar}/^{39}\text{Ar}$ laser-probe experimental procedure

After coarse crushing, clean single grains of amphibole were separated under the binocular and rinsed with methanol and distilled water. They were packed in aluminum bags and irradiated for 70 h in the McMaster nuclear reactor (Canada) with different flux monitors including MMHb-1 ( $520.4 \pm 1.7$  Ma) and HD-B1 ( $24.21 \pm 0.32$  Ma). The following factors for nuclear isotope interference corrections were used:  $(^{36}\text{Ar}/^{37}\text{Ar})_{\text{Ca}} = 0.000254$ ;  $(^{39}\text{Ar}/^{37}\text{Ar})_{\text{Ca}} = 0.000651$ ;  $(^{40}\text{Ar}/^{39}\text{Ar})_{\text{k}} = 0.0156$ . After irradiation, the sam-

ples were placed on a Cu-holder inside a UHV gas extraction system and baked for 48 h at 200°C. Step-heating and total fusion experiments were conducted on single grains using a laser probe operating in the continuous or semi-pulsed mode [23]. The analytical device consists of: (a) a multi-line continuous 6 W argon-ion laser; (b) a beam shutter for selection of exposure times, typically 30 s for individual steps; (c) divergent and convergent lenses for selection of the beam diameter; (d) a small inlet line for the extraction and purification of gases and (e) a MAP 215-50 noble gas mass spectrometer. The gain between the Faraday cup and electron multiplier at 2 kV is close to 200. Mass discrimination on the multiplier was calculated on the basis of a  $^{40}\text{Ar}/^{36}\text{Ar}$  ratio of  $292.0 \pm 1.7$  measured on an atmospheric argon aliquot. Each analysis involves 5 min for gas extraction and cleaning and 15 min for data acquisition by peak switching from mass 40 to mass 36. System blanks were evaluated every three experiments and ranged from  $2 \times 10^{-12}$  cc for  $^{40}\text{Ar}$  to  $5 \times 10^{-14}$  cc for  $^{36}\text{Ar}$ . Age and error calculations were made according to McDougall and Harrison [24]. Results are reported in Table 1 and represented as age spectra (Fig. 2). The quoted errors represent one sigma deviation and do not include uncertainty on the monitor age and its  $^{40}\text{Ar}/^{39}\text{Ar}$  ratio. This uncertainty is only introduced in the errors reported on the plateau and total ages. Ca/K ratios are evaluated according to the relation:  $\text{Ca}/\text{K} = 1.82 \times ^{37}\text{Ar}/^{39}\text{Ar}$ .

### 2.2. Results

For each sample dated with the  $^{40}\text{Ar}/^{39}\text{Ar}$  laser-probe method, both step-heating and total fusion of single grains were performed to better constrain the validity of each age determination (Fig. 2). Two grains of amphibole from site RD19 yield plateau dates of  $116.2 \pm 4.2$  and  $121.2 \pm 4.6$  Ma, respectively, for samples RD19D and RD19H. Both samples display evidence of discordant and mainly younger ages in the first heating steps related to low Ca/K and high Cl/K ratios compared to those associated with the plateaus. The Ca/K plateau ratios are significantly different for the two amphiboles, respectively,

Table 1  
 $^{40}\text{Ar}/^{39}\text{Ar}$  laser probe results

Temperature (°C)	$^{40}\text{Ar}^*/^{39}\text{Ar}$	$^{36}\text{Ar}/^{40}\text{Ar} \times 1000$	$^{39}\text{Ar}/^{40}\text{Ar}$	$^{37}\text{Ar}/^{39}\text{Ar}$	$^{39}\text{Ar}$ (%)	Age $\pm$ 1S.D.
<i>RD19D amphibole</i>				$J = 0.016844$		
430	4.775	3.282	0.0063	5.666	0.8	139.6 $\pm$ 89.5
540	4.036	2.813	0.0416	6.343	1.6	118.7 $\pm$ 68.5
610	2.65	2.904	0.0534	3.908	2.1	78.8 $\pm$ 74.3
720	1.761	3.035	0.0585	5.349	3.5	52.7 $\pm$ 42.3
850	2.651	1.639	0.1944	17.058	20.0	78.8 $\pm$ 4.1
855	3.363	0.55	0.2489	18.895	25.0	99.4 $\pm$ 13.5
885	3.107	0.336	0.2898	18.811	28.1	92.0 $\pm$ 34.0
920	3.343	1.206	0.1923	18.501	39.5	98.8 $\pm$ 11.6
1000	3.956	0.751	0.1966	17.846	67.5	116.4 $\pm$ 7.2
1025	3.862	1.007	0.1817	18.229	79.2	113.7 $\pm$ 7.8
1250	3.999	1.459	0.1421	19.633	100.0	117.6 $\pm$ 4.6
Fusion				Total age = 105.7 $\pm$ 8.5		
	4.226	1.672	0.1196	17.724	100.0	124.1 $\pm$ 2.5
<i>RD19H amphibole</i>				$J = 0.016844$		
500	2.676	3.321	0.0068	10.462	0.4	79.6 $\pm$ 298.3
625	4.794	2.795	0.0363	11.209	1.6	140.1 $\pm$ 87.1
785	5.001	3.059	0.0192	16.348	2.2	145.9 $\pm$ 168.2
825	2.627	1.731	0.1859	31.234	3.7	78.1 $\pm$ 55.5
855	4.259	1.584	0.1248	37.548	23.0	125.0 $\pm$ 7.4
900	4.026	1.103	0.1673	38.450	45.5	118.4 $\pm$ 11.6
925	3.768	0.964	0.1897	39.685	49.7	111.0 $\pm$ 33.9
955	3.985	0.678	0.2006	37.017	53.5	117.2 $\pm$ 30.4
1000	4.218	0.612	0.1940	36.578	60.1	123.8 $\pm$ 10.5
1050	4.057	0.713	0.1944	33.353	67.4	119.3 $\pm$ 14.0
1250	4.182	0.638	0.1939	37.096	100.0	122.8 $\pm$ 6.6
Fusion				Total age = 120.8 $\pm$ 4.9		
	3.898	1.508	0.1422	28.328	100.0	114.7 $\pm$ 4.0
<i>RD20 amphibole (1)</i>				$J = 0.014548$		
1	332.967	1.951	0.0012	29.563	0.3	3185 $\pm$ 397
2	28.927	3.041	0.0034	21.451	0.9	634 $\pm$ 350
3	29.389	2.725	0.0066	26.974	1.4	642 $\pm$ 297
4	3.401	3.163	0.0190	16.139	2.9	87 $\pm$ 195
5	7.371	2.542	0.0337	14.225	3.9	184 $\pm$ 161
6	3.898	2.832	0.0416	65.831	15.3	99.5 $\pm$ 16.4
7	4.009	2.393	0.0730	88.789	27.4	102.3 $\pm$ 16.5
8	4.108	2.078	0.0939	78.337	45.0	104.7 $\pm$ 13.2
9	4.392	1.739	0.1106	60.421	65.4	111.7 $\pm$ 14.5
10	4.856	1.822	0.0950	76.749	100.0	123.2 $\pm$ 7.8
				Total age = 145.8 $\pm$ 8.0		
<i>RD20 amphibole (2)</i>				$J = 0.014548$		
1	22.345	3.187	0.0026	26.444	1.3	508 $\pm$ 100
2	11.567	2.846	0.0137	16.695	1.9	281 $\pm$ 89
3	5.907	2.745	0.0319	34.310	4.4	149 $\pm$ 45
4	3.185	2.756	0.0582	72.228	22.7	81.7 $\pm$ 12.7
5	2.925	2.408	0.0985	78.199	30.9	75.2 $\pm$ 19.0
6	3.761	2.065	0.1035	61.879	50.3	96.1 $\pm$ 8.7
7	4.125	2.060	0.0947	68.612	100.0	105.2 $\pm$ 8.7
Fusion				Total age = 104.9 $\pm$ 7.3		
	4.124	2.437	0.0678	80.134	100.0	105.1 $\pm$ 13.6

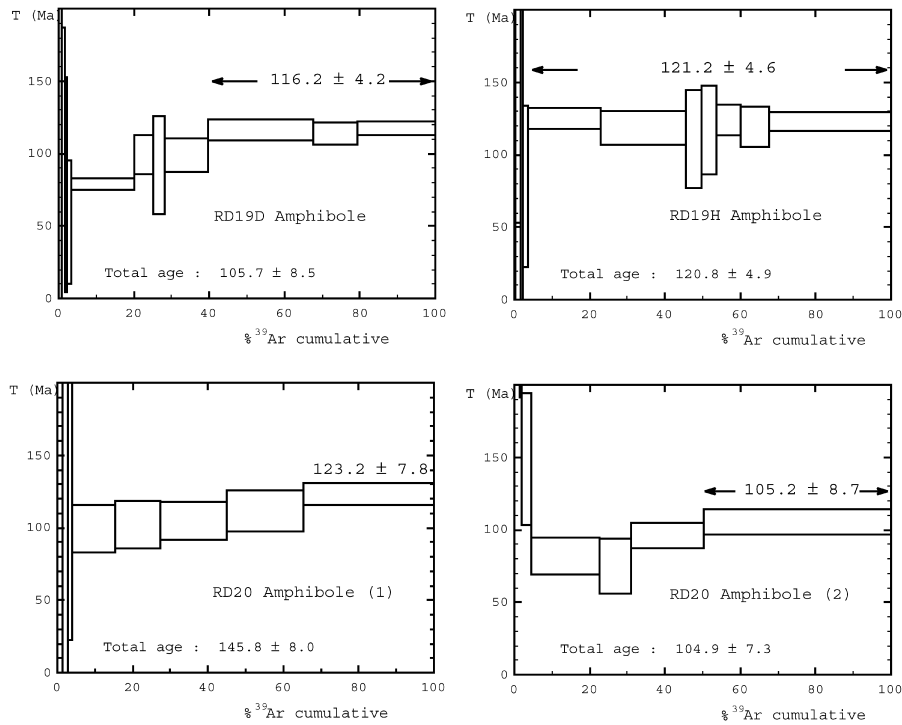


Fig. 2. Age spectra obtained on single amphibole grains from samples RD19 and RD20.

close to 33 and 68, which suggests that the dredged gabbros show some chemical variations. A plot of the isotopic data in  $^{36}\text{Ar}/^{40}\text{Ar}$  versus  $^{39}\text{Ar}/^{40}\text{Ar}$  correlation diagram yields intercept ages, respectively, of  $114.3 \pm 2.3$  and  $121.8 \pm 2.7$  Ma with atmospheric  $^{40}\text{Ar}/^{36}\text{Ar}$  initial ratios. The complete fusion of single grains gives ages of  $124.1 \pm 2.5$  Ma and  $114.7 \pm 4.0$  Ma. For sample site RD20, two grains of amphibole have been successively step-heated. The corresponding age spectra displays similar trends characterized by a progressive increase of apparent ages during incremental heating. Minimum ages are in the range 80–100 Ma and reach a maximum of  $123.2 \pm 7.8$  Ma for the oldest sample. Ca/K ratios are high compared to samples RD19, in the range 113–149. The high Ca contribution in these amphiboles has resulted in a large nuclear interference correction on the  $^{36}\text{Ar}$  measured by mass spectrometry, and by consequence in a significant error margin on the age. A third single grain from

this gabbro has yielded a direct fusion age of  $105.1 \pm 13.6$  Ma which remains compatible with  $^{40}\text{Ar}/^{39}\text{Ar}$  dates.

These new  $^{40}\text{Ar}/^{39}\text{Ar}$  ages on two gabbro sites dredged in the Huatung Basin indicate the existence of Early Cretaceous oceanic crust east of Taiwan. The different amphibole age spectra are partially discordant, probably as a result of some hydrothermal alteration on the oceanic floor. This effect is more pronounced in amphiboles from RD20 that do not display any plateau date, but discordant ages in the range 80–123 Ma. However, there is no record of younger dates which could suggest an Eocene age for the Huatung oceanic crust as supposed up to now. In addition, it must be stressed that the present data do not allow a distinction in cooling ages between the two sampling sites for which ages in the range 115–125 Ma can be retained. These ages are interpreted to record cooling of the gabbros at a temperature of 500–550°C [25,26].

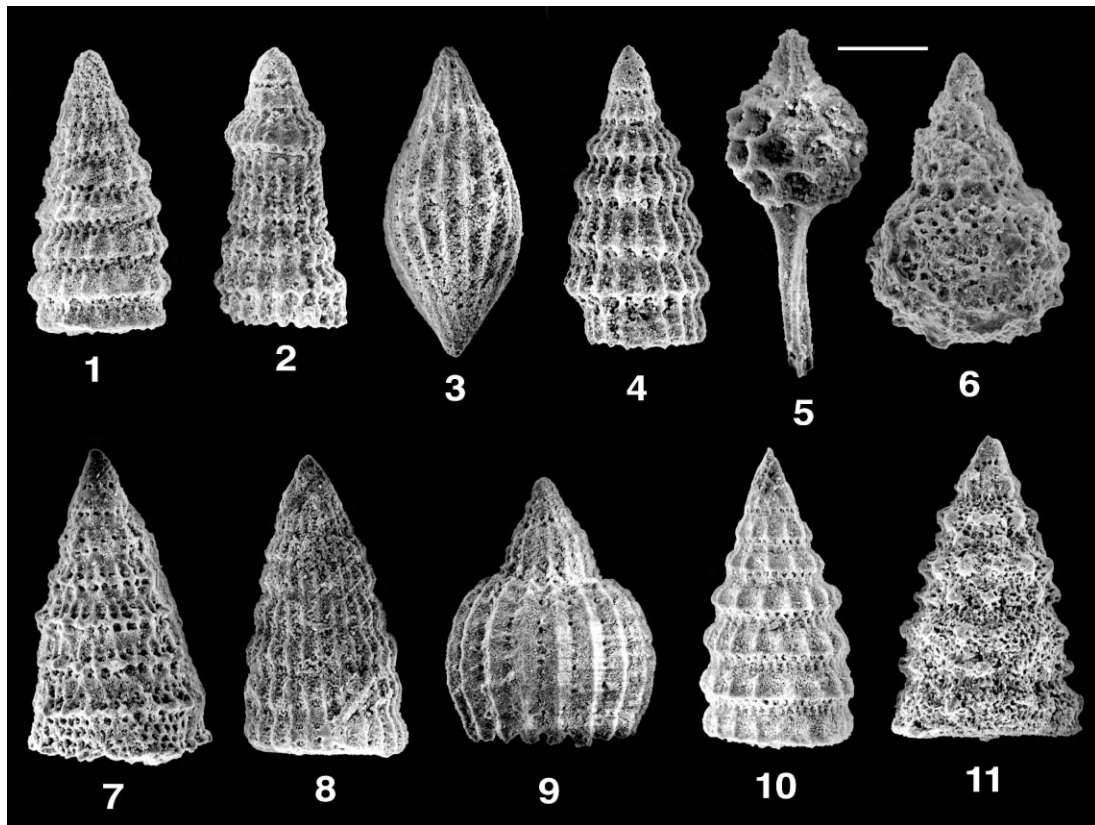


Plate 1. Representative Lower Cretaceous Radiolaria from Lanyu Island, Taiwan. Length of scale bar, upper right, equals number of micrometers cited for each illustration. Range of each species is cited from previous studies. (1) *Pseudodictyomitra carpatica* (Lozyniak) (scale = 66  $\mu\text{m}$ ). Range: upper Tithonian to Barremian. (2) *Dictyomitra koslovae* Foreman (scale = 70  $\mu\text{m}$ ). Range: Barremian to Santonian. (3) *Archaeodictyomitra lacrimula* (Foreman) (scale = 70  $\mu\text{m}$ ). Range: lower Berriasian to lower Aptian. (4) *Dictyomitra duodecimcostata* (Squinabol) (scale = 88  $\mu\text{m}$ ). Range: Barremian to Santonian. (5) *Pantanellium masirahense* Dumitrica (scale = 44  $\mu\text{m}$ ). Range: Hauterivian to lower upper Barremian. (6) *Clavaxitus* sp. A (scale = 51  $\mu\text{m}$ ). Range: Valanginian to Barremian. (7) *Pseudocrolanium flügeli* Jud (scale = 66  $\mu\text{m}$ ). Range: Barremian. (8) *Archaeodictyomitra leptocostata* (Wu and Li) (scale = 94  $\mu\text{m}$ ). Range: upper Valanginian to lower upper Barremian. (9) *Thanarla pulchra* (Squinabol) (scale = 70  $\mu\text{m}$ ). Range: upper Berriasian to lower Aptian. (10) *Pseudodictyomitra lanceoloti* Schaaf (scale = 66  $\mu\text{m}$ ). Range: lower to lower upper Barremian. (11) *Xitus normalis* (Wu and Li) (scale = 94  $\mu\text{m}$ ). Range: Hauterivian to Barremian.

### 3. Paleontological ages on radiolarian assemblages from the Luzon Arc

Radiolarians have been discovered in several red chert float samples in an area located north of the Yehyu Creek, northern Lanyu Island (Luzon Arc) (Fig. 1). The size of the samples ranges from a few centimeters to tens of centimeters. They are mostly red in color due to the oxidation of hematite inclusions. Each piece of float can be a single fragment from one bedded chert, or a breccia with disordered bedded cherts. About

50 species of radiolarians have been recognized (Yeh and Cheng, Early Cretaceous Radiolarians from the Philippine Plate, Bulletin of National Museum of Natural Science, in preparation). Eleven representative species are shown in Plate 1. The co-occurrence of these forms indicates that the Lanyu red cherts were deposited in the Early Cretaceous, and have a Barremian age of about 115 Ma according to the time scale of IUGS 1989.

The cherts are found isolated from the other volcanic rocks (Tungchin andesites) which cover the northern part of the island. The relationship

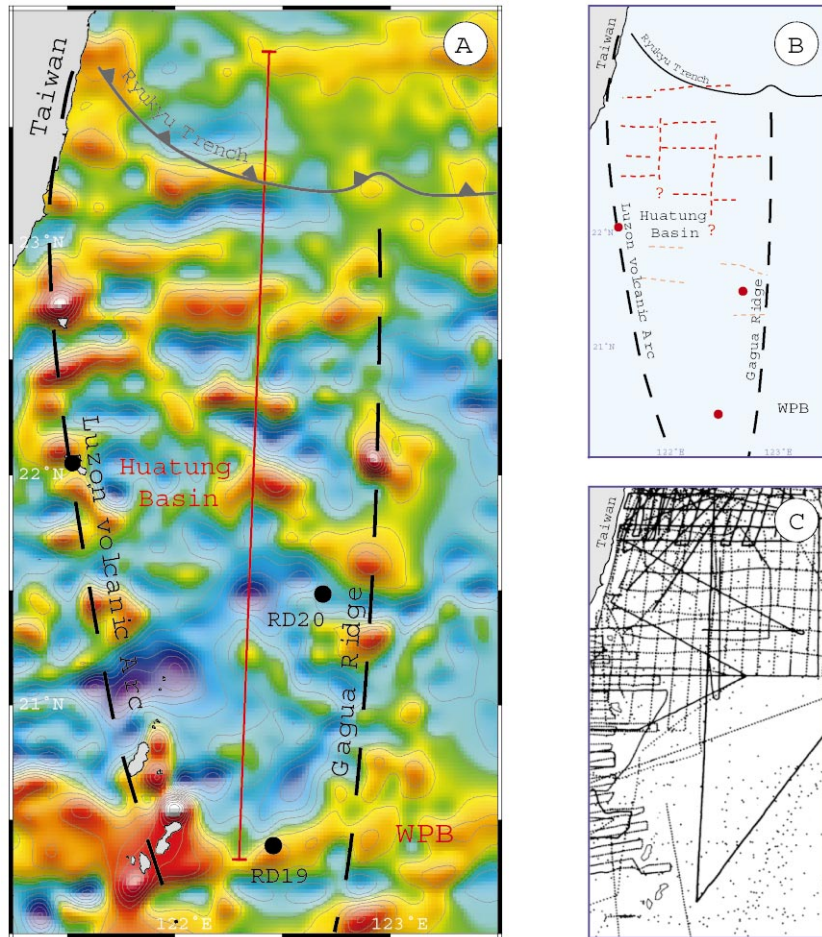


Fig. 3. (A) Magnetic map of the Huatung Basin with the location of the N-S magnetic profile (in red) which is used to perform magnetic identifications in our study. Major tectonic features have been localized. Black circles correspond to sampling sites. (B) Trends of the positive magnetic anomalies and fracture zones. (C) Ship tracks of all magnetic surveys that have been conducted in this area.

between these cherts and the other rocks is therefore not clear but we believe that they may have been carried out during the eruption of Tungchin Andesite, probably during the Cenozoic. Radiolarians are the only fossils found in pelagic sedimentary rocks, such as mudstones and cherts, which have been deposited in basins at low latitudes and below Carbonate Compensation Depth. There is no doubt that radiolarian cherts are oceanic in origin and very possibly from basins of great depth. We believe that these Cretaceous cherts are fragments of the former oceanic plate on which the Luzon Arc was built since Late Oli-

ocene time [9]. The presence of these assemblages supports the Early Cretaceous ages revealed by Ar/Ar measurements for the oceanic crust of the Huatung Basin.

## 4. Geophysical study of the Huatung Basin

### 4.1. Magnetism

The geomagnetic data shown on Fig. 3 were acquired mainly during the ACT cruise in 1996 [27] and the EW9509 cruise in 1995 [28]. These

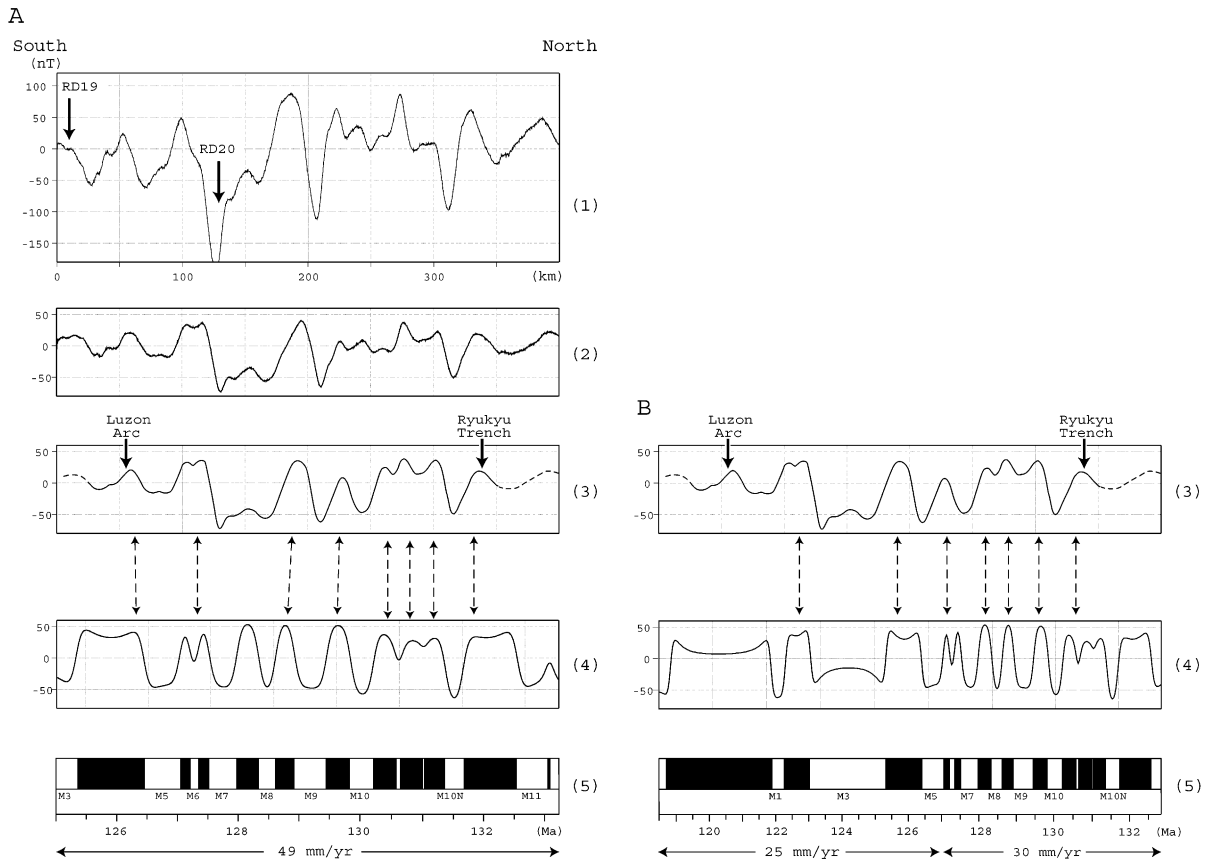


Fig. 4. Identification of the magnetic lines. (A) Spreading rate = 49 mm/yr: (A1) original data; (A2) 60° phase-shifted original profile; (A3) 60° phase-shifted original profile, stacked with N–S magnetic profiles acquired during the ACT cruise in the Huatung Basin; (A4) synthetic profile with a spreading rate of 4.9 cm/yr; (A5) 125 to 133 Ma time scale (see Table 1). (B) Spreading rate range between 25 and 30 mm/yr: (B3) same as A3; (B4) synthetic profile with a spreading rate varying between 25 and 30 cm/yr; (B5) 118.5 to 133 Ma time scale (see Table 1).

data were completed with data acquired between 1967 and 1997 during several other cruises [20]. More recently (1997) a N–S magnetic profile was acquired during the cruise ORI495 across the whole length of the Huatung Basin. It runs in a direction parallel to the major fracture zones. We used this profile corrected in its northern part by the stack of N–S ACT magnetic lines to identify magnetic anomalies in the basin and to date more precisely the spreading phase.

On the magnetic anomaly map (Fig. 3), the Huatung Basin presents several E–W trending well-defined magnetic polarity reversals between latitudes 21.7°N and 23.6°N. The existence of two N–S trending fracture zones at longitudes

121.8°E and 122.4°E is confirmed by seismic reflection profiles [13,20]. The absence of E–W trending magnetic anomalies south of 21.7°N is probably due to the lack of data in this area since a recent N–S magnetic profile acquired between 25°N and 20.5°N reveals well-marked magnetic anomalies (Fig. 4A1). The NW–SE positive magnetic anomaly observed between latitudes 21.5° and 22.5° does not seem to be a significant feature, since on seismic-reflection profiles (Fig. 5), it does not correlate with any feature of the basement in the Huatung Basin. We suppose that this NW–SE anomaly is due to the dextral offset of an E–W positive anomaly by two N–S fracture zones [20] (Fig. 3). Moreover, this anomaly is not well-



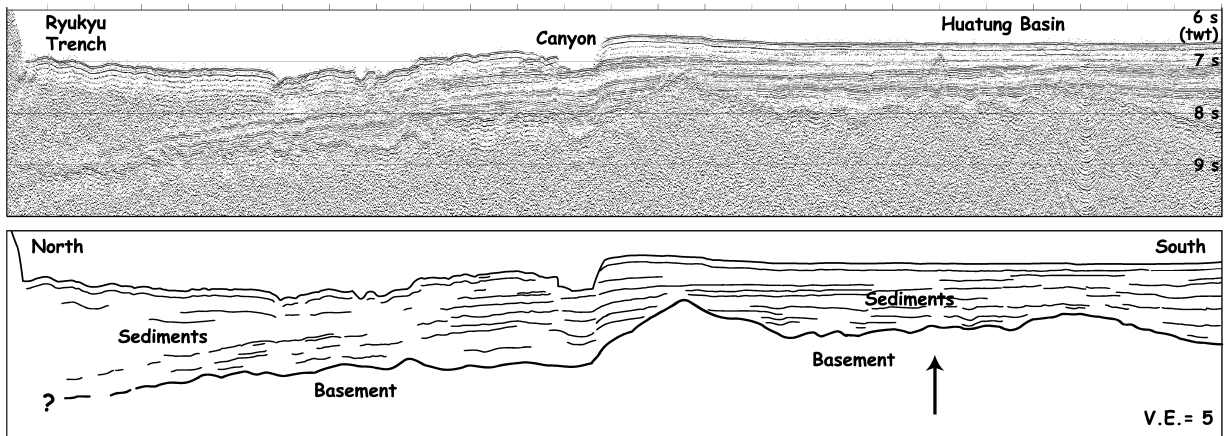


Fig. 5. N–S ACT seismic profile across the Huatung Basin (Fig. 1C). The vertical arrow indicates the boundary between a northern domain where E–W magnetic anomalies are well expressed and a southern domain where E–W anomalies do not appear (see Fig. 3).

constrained since it lies at the limit between a northern domain of the Huatung Basin where magnetic data are abundant and a southern domain where data are scarce.

We present a new magnetic anomaly identification of the magnetic polarity reversals observed on this profile (Fig. 4). As a first step, we have examined an extensive set of magnetic anomaly models generated with various spreading rates and times of spreading onset and cessation within the Cretaceous. We assume a 3 km-thick magnetized layer with a top at 6.2 km below sea level which is the average depth of the oceanic basement in the Huatung Basin. Magnetization is set to  $\pm 8$  A/m. The geomagnetic polarity time scale of Kent and Gradstein [29] is used throughout this study (Table 2). We consider that the basin opened in a N–S direction, parallel to the fracture zones and perpendicular to the magnetic anomalies. More than 50 synthetic profiles were computed using spreading ages ranging from 140 to 118 Ma (the beginning of the ‘Cretaceous Long Normal-Polarity Chron’). The observed profile collected in the Huatung Basin was phase-shifted in  $20^\circ$  increments based on the theory of Schouten and McCamy [30]. Phase shifting of the anomalies can remove the effects of the depth, thickness, scale and the skewing effect of the magnetization and of the earth’s field direction for easier comparison and identification of anomalies. The re-

sulting observed profiles were finally compared with each synthetic profile.

We found two good fits. The first model (Fig. 4A) suggests that the basin formed between 132 and 126 Ma with a constant half spreading rate of 4.9 cm/yr. The ages of the basin inferred from this first model are a little older than ages revealed by the Ar/Ar measurements. The second model (Fig. 4B) seems to indicate that the basin formed between 131 and 119 Ma with a half spreading rate of 3 cm/yr between 131 and 127 Ma and of 2.5 cm/yr between 127 and 119 Ma. We favor this

Table 2

Magnetic reversal time used in this study after Kent and Gradstein [29]

Normal polarity intervals (Ma)	Anomaly (reversed polarity)
118.7–121.81	M0
122.25–123.03	M1
125.36–126.46	M3
127.05–127.21	M5
127.34–127.52	M6
127.97–128.33	M7
128.60–128.91	M8
129.43–129.82	M9
130.19–120.57	M10
130.63–131.00	
131.02–131.36	
131.65–132.53	M10N
133.03–133.08	M11

second solution which is in better accordance with Ar/Ar and paleontological ages. In both cases, we found that the age of the basin increases towards the north, which means that the spreading center was located south of the actual basin. The best fits are obtained when the observed profile is phase-shifted by about 60°, which suggests that the basin formed in the northern hemisphere.

#### 4.2. Depth and thickness of the oceanic basement in the Huatung Basin

From the analysis of the seismic reflection profiles, the oceanic basement in the Huatung Basin appears to be 6.2 km deep on average [13,20]. The basement is overlain by sediments with an average thickness of 1.4 km (Fig. 5). If we take account of the 700 m subsidence of the basement due to the sediment load, the original depth of the oceanic basement in the basin (free of sediments) was probably about 5500 m. The relation: depth (m) =  $6400 - 3200e^{-(t(\text{Ma})/62.8)}$  of Parsons and Sclater [31] for ocean floor older than 70 Ma gives a theoretical depth of about 5900 m for the roughly 125–130 Ma-old oceanic basement of the Huatung Basin. The basement of the basin therefore displays a mean depth which is 400 m shallower than the calculated depth.

Furthermore, the crust of the Huatung Basin

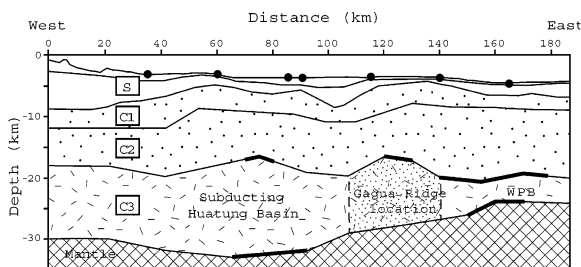


Fig. 6. Crustal velocity model around latitude 23°50'N from McIntosh and Nakamura [33]. (section D, Fig. 1). Layers S represents sediments. Layers C1 ( $v=5\text{--}5.8$  km/s) and C2 ( $v=6\text{--}6.6$  km/s) represent the seaward extension of the Ryukyu Arc crust. The nature of crustal layer C3 is not well determined but on the basis of intersecting N–S velocity models, it likely represents the subducting PSP [33]. Black circles are the location of OBS stations. The heavy lines mark reflection points for arrivals used to constrain the top and bottom of C3.

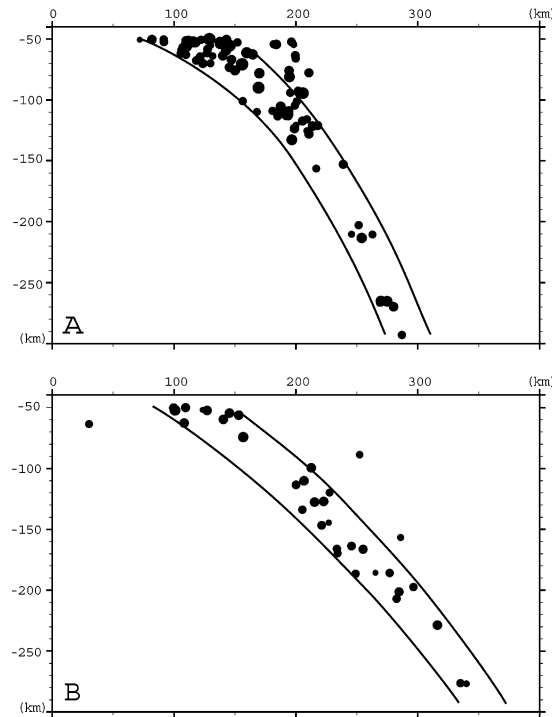


Fig. 7. N–S vertical sections with relocated ISC [34] hypocenters. (A) N–S section made west of the Gagua Ridge. (B) Section performed east of the Gagua Ridge. See Fig. 1 for locations.

has an abnormal thickness. A NW–SE OBS (ocean bottom seismometers) line across the Huatung Basin has revealed a thickness of about 10 km for the crust [32]. Another E–W line of OBS data acquired beneath the Ryukyu forearc basins (Figs. 1 and 6) shows that the subducting plate thickens significantly towards the west [33]. The velocity model (Fig. 6) shows that the subducting oceanic crust east of the Gagua Ridge is unusually thin (about 5 km) in good agreement with previous refraction studies on the PSP [7], and by contrast is unusually thick (about 10–15 km) west of the Gagua Ridge.

#### 4.3. Analysis of the seismicity

We have examined the intraplate seismicity in the Ryukyu region in order to visualize the seismic slab which is subducting northward beneath the Ryukyu Arc. Earthquake data in the study

area were obtained from Engdahl et al. [34], who have improved the hypocenter locations from the International Seismological Centre (ISC) Catalog. This database was used to calculate the depth of the Wadati–Benioff zone beneath the Ryukyu Trench. Two different regions, with distinct patterns of seismicity, are observed west and east of the Gagua Ridge at longitude 123°E. Two N–S cross-sections based on the seismicity illustrate the significant difference of the dip of the slab in these two regions (see Fig. 1, sections A and B).

The N–S section west of the Gagua Ridge (Fig. 7A) shows a steep 65°-dipping Wadati–Benioff zone down to a depth of about 300 km, in good agreement with earlier seismological results [35]. The section east of the Gagua Ridge (Fig. 7B) shows a more moderate 50°-dipping Wadati–Benioff zone down to a depth of about 280 km.

These seismological observations could be simply explained by a westward increase of the density of the lithosphere being subducted beneath the Ryukyu Trench. This density variation could reflect the difference in age of the subducting lithosphere. West of the ridge, the steep-dipping Wadati–Benioff zone might characterize the subduction of an Early Cretaceous slab whereas the gently-dipping Wadati–Benioff zone observed east of 123°E would reflect the subduction of a Middle Eocene oceanic plate.

#### 4.4. Details of the basement from seismic reflection profiles

Numerous N–S seismic-reflection profiles were acquired during the ACT cruise [27] in the Huatung Basin. One profile is shown on Fig. 5. The oceanic basement appears to be generally smooth, except near the Taitung Canyon where a depression of the top of the basement has been described by Schnurle et al. [36]. The height of the abyssal hills does not exceed 250 m, with an average value of 50 m. The overall relief of abyssal hills can be related to seafloor spreading rates: large relief or rough topography is associated with slow spreading rates and smooth topography with faster spreading rates [37,38]. We therefore suggest that the regular topography of the basement and its relatively smooth relief is related to a

fairly fast and relatively constant spreading rate, which is entirely consistent with the full spreading rate of about 5 to 6 cm/yr deduced from our magnetic anomalies model.

## 4. Discussion

$^{40}\text{Ar}/^{39}\text{Ar}$  dating of gabbros collected in the Huatung Basin suggests that the oceanic crust of the basin could be Early Cretaceous in age (115–125 Ma). These results are in good agreement with Early Cretaceous (115 Ma) radiolarian assemblages from the Lanyu island which probably indicate an Early Cretaceous oceanic basement underlying the volcanic Luzon Arc.

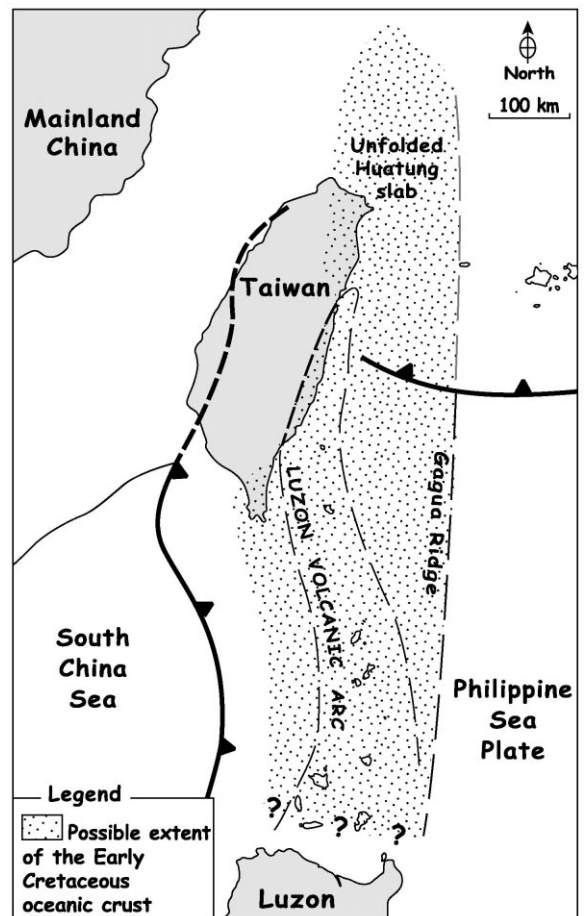


Fig. 8. Diagram showing the possible extension of the Early Cretaceous crust, based on the sections with hypocenter locations and the geology of the area.

Our analysis of the magnetic polarity reversals in the Huatung Basin differs from previous analyses. We favor ages between 131 and 119 Ma for the basin crust. These ages are in accordance with ages revealed by geochronological and paleontological data. The best fit for our model of magnetic anomalies corresponds to an opening of the basin at an average full rate of 5–6 cm/yr from a spreading center which would have been located to the south of the current basin. This suggests that the oceanic crust flooring the Huatung Basin constituted a larger basin than currently observed (Fig. 8) and that only a piece of its northern part has been trapped by the PSP.

From these observations, the N–S Gagua Ridge appears to represent a suture between two lithospheres of different age. The WPB east of the ridge is Middle Eocene in age [8] and the Huatung Basin west of the ridge is Early Cretaceous in age. This difference of age is supported by a significant variation in the dip of the subducting slab beneath the Ryukyu Trench, probably related to the increase of the density of the subducting lithosphere with increasing age.

The old age of the Huatung Basin versus a younger age of the WPB could be confirmed by strain patterns observed in the downgoing slab. Kao et al. [39] have indeed noted that a change of strain patterns within the subducting slab occurs in a very narrow zone between 123°E and 124°E, in the vicinity the Gagua Ridge. Surprisingly, west of the Gagua Ridge, extensional events at depths between 80 and 120 km and downdip compression at 270 km within the subducting plate have been observed, in contrast to observations made along the rest of the Ryukyu Arc. Within a given segment, such a co-existence of downdip extensional strain and downdip compressional events can be correlated with either an older age of the downgoing slab or a slower rate of convergence [40]. As there is no variation of the rate of convergence across the Gagua Ridge, it seems likely that the abnormal strain patterns observed within the subducting plate west of the Gagua Ridge are the consequence of the greater age of the Huatung Basin (Kao, personal communication).

The depth of the Huatung Basin appears to be

shallower than the theoretical depth. However, OBS data have shown that the crust of the basin is 10 to 15 km thick, which is greater than a normal oceanic crust ( $\sim 6$  km). A high supply of magma could explain the abnormal thickness and depth of the basin crust.

Finally, our results show that the Huatung Basin is a trapped piece of an Early Cretaceous ocean or back-arc basin. If so, the Gagua Ridge acted as a plate boundary. Strike-slip deformation has occurred along it, as shown by the set of N–S linear ridges and troughs [13]. The WPB is considered to have formed in the southern hemisphere [1] and has recorded strong northward motion (20°) and clockwise rotation ( $> 80^\circ$ ) since its formation [41]. We suggest that because of its important northward motion, the WPB came into contact by the way of strike-slip motion along what would become the Gagua Ridge with an old ocean floor created in the northern hemisphere. The possible extent of the Early Cretaceous crust is shown on Fig. 8. A good candidate for this old crust could be the proto-south China Sea (PSCS) [42] that would have been trapped by the Manila subduction zone. The PSCS is indeed supposed to have formed in the northern hemisphere during the Mesozoic, which is in good agreement with our results. Another candidate for the origin of the Huatung Basin could possibly be the Mesozoic ‘New Guinea Basin’ (NGB) [43]. The ophiolitic substratum of various ages from the Late Jurassic to the Early Cretaceous that extends from the Northern Sierra Madre (Luzon) to Eastern Halmahera [12] (Fig. 1) could also be relicts of the NGB and therefore have the same origin as the Huatung Basin. However, the NGB [43] as well as the ophiolites of Eastern Philippines [42] are considered to have been formed near the equator or in the southern hemisphere during the Mesozoic, which is not compatible with our magnetic anomalies modeling results.

## 5. Conclusion

Ar/Ar dating, micropaleontological data and geophysical study of the Huatung Basin show

that the basin crust is Early Cretaceous in age. However, some points remain unclear. We have no constraint on the time of the onset and cessation of spreading in the Huatung Basin: the northern part of the basin has indeed been subducting beneath the Ryukyu Trench for several millions years. The Luzon arc has developed on the southern part of the Huatung Basin, trapping only a small part of the Cretaceous seafloor. Thus, the initial shape of the basin remains unknown. Moreover, the old age of the basin needs to be confirmed with ocean drilling in the northern part of the Huatung Basin, dredges on both flanks of the northern part of the Gagua Ridge or through heat flow measurements in the central part of the basin. Acquisition of paleomagnetic data in the basin could contribute to understanding its behavior with respect to the other major plates since the Early Cretaceous time. Finally, geochemical studies on the gabbro samples from the Huatung Basin will be done in order to determine whether the Early Cretaceous crust formed in an ocean or in a back-arc context.

### Acknowledgements

Many thanks to Steve Lewis and Cindy Evans for their help in obtaining the samples which were dredged during the *Vema* cruise and for providing us their previous K/Ar results. Support for the curating facilities of the Lamont–Doherty Geological Observatory Deep-Sea Sample Repository is provided by the National Science Foundation through Grant OCE97-11316 and the Office of Naval Research through Grant N00014-96-1-0186. Thanks to Philippe Schnürle and Yvonne Font for processing seismic profile. Discussion of the results with Chao-Shing Lee, Tan Kin Wang, Honn Kao and Jean-Claude Sibuet were very helpful. The manuscript was improved by reviews from C. Evans, R. Hall and J. Malod. Figs. 1, 2 and 5 were produced using Wessel and Smith's GMT software. [AC]

### References

- [1] T.W.C. Hilde, C.-S. Lee, Origin and evolution of the West Philippine Basin, *Tectonophysics* 102 (1984).
- [2] K. Okino, S. Kasuga, Y. Ohara, A new scenario of the Parece Vela basin genesis, *Mar. Geophys. Res.* 20 (1998) 21–40.
- [3] D. Hussong, S. Uyeda, Tectonic processes and the history of the Mariana arc: a synthesis of the results of Deep Sea Drilling Project Leg 60, in: M. Lee, R. Powell (Eds.) *Init. Reports DSDP 60*, vol. 60, National Science Foundation, Washington, DC, 1981, pp. 909–929.
- [4] T. Seno, S. Stein, A.E. Gripp, A model for the motion of the Philippine sea Plate consistent with NUVEL-1 and geological data, *J. Geophys. Res.* 98 (1993) 17941–17948.
- [5] C.S. Lee, T. Hilde, Magnetic lineations in the western Philippine Sea, *Acta Oceanogr. Taiwanica* 1 (1971) 69–76.
- [6] T.C. Shih, Marine magnetic anomalies from the western Philippine Sea: implications for the evolution of marginal basins, in: D.E. Hayes (Ed.), *The Tectonic and Geologic Evolution of Southeast Asia Seas and Islands*, *Geophys. Monogr.*, Am. Geophys. Union, vol. 23, 1980, pp. 49–75.
- [7] S. Murauchi, N. Den, S. Asana, H. Hotta, T. Yoshii, T. Asanuma, K. Hagiwara, T. Sato, W.J. Ludwig, J.I. Ewing, N.T. Edgar, R.E. Houtz, Crustal structure of the Philippine Sea, *J. Geophys. Res.* 73 (1968) 3143–3171.
- [8] D.E. Karig, J.C. Ingle et al., *Initial reports of the Deep Sea Drilling Project*, U.S. Government Printing Office, vol. 31, Washington, DC, 1975.
- [9] M.A. Richard, H. Bellon, R.C. Maury, E. Barrier, W.-S. Juang, Miocene to recent volcanism in eastern Taiwan K-Ar ages and petrography, *Tectonophysics* 125 (1986) 87–102.
- [10] T.F. Yang, T. Lee, C.-H. Chen, S.-N. Cheng, U. Knittel, R.S. Punongbayan, A.R. Rasdas, A double island arc between Taiwan and Luzon consequence of ridge subduction, *Tectonophysics* 258 (1996) 85–101.
- [11] D.E. Karig, Accreted terranes in the northern part of the Philippine archipelago, *Tectonics* 2 (1983) 211–236.
- [12] S.D. David, *Géologie du sud-est de Luzon*, Ph.D. thesis, Université de Nice-Sophia Antipolis, No. 21, 1994 (in English).
- [13] A. Deschamps, S. Lallemand, J.-Y. Collot, A detailed study of the Gagua Ridge: a fracture zone uplifted during a plate reorganisation in the Mid-Eocene, *Mar. Geophys. Res.* 20 (1998) 403–423.
- [14] J.L. LaBrecque, D.V. Kent, S.C. Cande, Revised magnetic polarity time scale for late Cretaceous and Cenozoic time, *Geology* 5 (1977) 330–335.
- [15] S.C. Cande, D.V. Kent, Revised calibration of the geomagnetic polarity timescale for the Late Cretaceous and Cenozoic, *J. Geophys. Res.* 100 (1995) 6093–6095.
- [16] H.-M. Kao, C.-S. Lee, S.-K. Hsu, C. Wang, Magnetic ages in the East and South of Taiwan offshore areas and its possible tectonic evolution, abstract in SEASIA Conference, May 9–12th, Montpellier, France, 1999, pp. 277–279.

- [17] C.-S. Lee, S.-K. Hsu, K. Okino, K. Tamaki, Deep Drag Ocean Bottom Magnetometer and its application on the Tertiary Magnetic Isochrons, Abstract in Geophysical Meeting, Keelung, October 28–29th, 1999.
- [18] R. Hall, J.R. Ali, C.D. Anderson, Cenozoic motion of the Philippine Sea Plate Paleomagnetic evidence from eastern Indonesia, *Tectonics* 14 (1995) 1117–1132.
- [19] J.-C. Sibuet, S.-K. Hsu, X. Le Pichon, J.-P. Le Formal, D. Reed, G. Moore, C.-S. Liu, Philippine Sea Plate and Taiwan Sea Plates: Formation of Taiwan, Abstract in SEASIA Conference, May 9–12th, Montpellier, France, 1999, p. 21.
- [20] S.-K. Hsu, C.-S. Liu, C.-T. Shyu, S.-Y. Liu, J.-C. Sibuet, S. Lallemand, C. Wang, D. Reed, New gravity and magnetic anomaly maps in the Taiwan-Luzon region and their preliminary interpretation, *TAO 9* (1998) 509–532.
- [21] C.L. Mrozowski, S.D. Lewis, D.E. Hayes, Complexities in the tectonic evolution of the West Philippine Basin, *Tectonophysics* 82 (1982) 1–24.
- [22] C.A. Evans, S.D. Lewis, The tectonic significance of the Gagua Ridge, Luzon-Taiwan region, *Eos, Trans. Am. Geophys. Union* 65 (1984) 1132.
- [23] P. Monié, R. Caby, M.H. Arthaud, The Neoproterozoic brasiliano orogeny of Northeast Brazil.  $40\text{Ar}$ – $39\text{Ar}$  ages and petro-structural data from Ceara, *Precamb. Res.* 81 (1997) 241–264.
- [24] I. McDougall, T.M. Harrison, *Geochronology and Thermochronology by the  $40\text{Ar}/39\text{Ar}$  Method*, Oxford University Press, New York, 1988.
- [25] T.M. Harrison, Diffusion of  $40\text{Ar}$  in hornblende, *Contrib. Mineral. Petrol.* 78 (1981) 324–331.
- [26] P.S. Dahl, The effects of composition on retentivity of argon and oxygen in hornblende and related amphiboles: a field-tested empirical model, *Geochim. Cosmochim. Acta* 60 (1996) 3687–3700.
- [27] S. Lallemand, C.-S. Liu, ACT Scientific Crew, Swath bathymetry mapping reveals details of the active arc-continent collision offshore Taiwan, *EOS Trans.* 78(17) (1997) AGU, 173–175.
- [28] C.-S. Liu, D.L. Reed, N. Lundberg, G.F. Moore, K.D. McIntosh, Y. Nakamura, T.K. Wang, T.H. Chen, S. Lallemand, Deep seismic imaging of the Taiwan arc-continent collision zone, Abstract AGU Fall Meeting, Dec. 11–15, 1995, San Francisco.
- [29] D.V. Kent, F.M. Gradstein, A Cretaceous and Jurassic geochronology, *Geol. Soc. Am. Bull.* 96 (1985) 1419–1427.
- [30] H. Schouten, K. McCamy, Filtering marine magnetic anomalies, *J. Geophys. Res.* 77 (1972) 7089–7099.
- [31] B. Parsons, J.G. Sclater, An analysis of the variation of the ocean floor bathymetry and heat flow with age, *J. Geophys. Res.* 82 (1977) 803–827.
- [32] Y.-S. Yang, T.K. Wang, Crustal velocity variation of the western Philippine Sea Plate from TAICRUST OBS/MCS line 23, *TAO 9* (1998) 379–393.
- [33] K.D. McIntosh, Y. Nakamura, Crustal structure beneath the Nanao forearc basin from TAICRUST MCS/OBS line 14, *TAO 9* (1998) 345–362.
- [34] E.R. Engdahl, R.D. van der Hilst, R. Buland, Global teleseismic earthquake relocation with improved travel times and procedures for depth relocation, *Bull. Seismol. Soc. Am.* 88 (1998) 722–743. Online data set (available from E. Robert Engdahl, USGS) via anonymous ftp: ftp 136.177.20.1 cd misc/engdahl/EHB compressed hypocenter data file 1964–1995 (EHB.HDF) and format description (FORMAT.HDF).
- [35] Y. Font, S. Lallemand, J. Angelier, Etude de la transition entre l'orogène actif de Taiwan et la subduction des Ryukyu: Apport de la sismicité, *Bull. Soc. Géol. France* 3 (1999) 271–283.
- [36] P. Schnurle, C.-S. Liu, S.E. Lallemand, D. Reed, Structural controls of the Taitung Canyon in the Huatung Basin east of Taiwan, *TAO 9* (1998) 453–472.
- [37] H.W. Menard, L.M. Dorman, Dependence of depth anomalies upon latitude and plate motion, *J. Geophys. Res.* 82 (1967) 5329–5335.
- [38] A.R. Pockalny, R.T. Bird, Late Cretaceous and Cenozoic seafloor and oceanic basement roughness; spreading rate, crustal age and sediment thickness correlations, *Earth Planet. Sci. Lett.* 123 (1994) 239–254.
- [39] H. Kao, S.J. Shen, K.F. Ma, Transition from oblique subduction to collision: earthquakes in the southernmost Ryukyu arc-Taiwan region, *J. Geophys. Res.* 103 (1998) 7211–7229.
- [40] H. Kao, W.-P. Chen, Earthquakes along the Ryukyu-Kyushu Arc: strain segmentation, lateral compression, and the Thermomechanical state of the plate interface, *J. Geophys. Res.* 96 (1991) 21443–21485.
- [41] R.B. Haston, M. Fuller, Paleomagnetic data from the Philippine Sea Plate and their tectonic significance, *J. Geophys. Res.* 96 (1991) 6073–6098.
- [42] R. Hall, Cenozoic plate tectonic reconstructions of SE Asia, in: Fraser, Matthews, Murphy (Eds.), *Petroleum Geology of Southeast Asia*, Geological Society Special Publication, No. 126, 1997, pp. 11–23.
- [43] M. Pubellier, J. Ali, C. Monnier, Cenozoic deformation at the margin of Eurasia, Australia and the Philippines: 'Hits and run' plate tectonics, Abstract in SEASIA Conference, May 9–12th, Montpellier, France, 1999, p. 33.
- [44] W.H.F. Smith, D.T. Sandwell, Global seafloor topography from satellite altimetry and ship depth soundings, *Science* 277 (1997) 1956–1962.